Absorption of lower hybrid waves in the scrape off layer of a diverted tokamak

Absorption of lower hybrid waves in the scrape off layer of a diverted tokamak

G. M. Wallace,[1] R. R. Parker,[1] P. T. Bonoli,[1] A. E. Hubbard,[1] J. W. Hughes,[1] B. L. LaBombard,[1] O. Meneghini,[1] A. E. Schmidt,[1] S. Shiraiwa,[1] D. G. Whyte,[1] J. C. Wright,[1] S. J. Wukitch,[1] R. W. Harvey,[2] A. P. Smirnov,[2] and J. R. Wilson[3]
[1]*MIT Plasma Science and Fusion Center, Cambridge, Massachusetts 02139, USA*
[2]*CompX, Del Mar, California 92014, USA*
[3]*Princeton Plasma Physics Laboratory, Princeton, New Jersey 08543, USA*

(Received 24 February 2010; accepted 11 June 2010; published online 20 August 2010)

The goal of the Lower Hybrid Current Drive (LHCD) system on the Alcator C-Mod tokamak [Hutchinson *et al.*, Phys. Plasmas **1**, 1511 (1994)] is to investigate current profile control under plasma conditions relevant to future tokamak experiments. Experimental observations of a LHCD "density limit" for C-Mod are presented in this paper. Bremsstrahlung emission from relativistic fast electrons in the core plasma drops suddenly above line averaged densities of 10^{20} m^{-3} ($\omega/\omega_{LH} \sim 3-4$), well below the density limit previously observed on other experiments ($\omega/\omega_{LH} \sim 2$). Electric currents flowing through the scrape off layer (SOL) between the inner and outer divertors increase dramatically across the same density range that the core bremsstrahlung emission drops precipitously. These experimental x-ray data are compared to both conventional modeling, which gives poor agreement with experiment above the density limit and a model including collisional absorption in the SOL, which dramatically improves agreement with experiment above the observed density limit. These results show that strong absorption of LH waves in the SOL is possible on a high density tokamak and the SOL must be included in simulations of LHCD at high density.
 [doi:10.1063/1.3465662]

I. INTRODUCTION

The Lower Hybrid Current Drive (LHCD) system[1] on the Alcator C-Mod tokamak[2] is designed to investigate current profile control under plasma conditions relevant to ITER (Ref. 3) and other future tokamaks. The efficiency of LHCD is predicted to scale with the inverse of the electron density,[4] however, LHCD experiments on many tokamaks[5–7] have observed a drop in efficiency steeper than $1/n_e$ above a critical density. The critical density associated with reduced current drive in C-Mod is unique in that it occurs at a value significantly lower than what would have been expected based on prior LHCD experiments. This paper presents experimental results and analysis from the Alcator C-Mod LHCD experiment suggesting that interactions between LH waves and the SOL plasma can have a substantial impact on the operational effectiveness of a LHCD system in high density ohmic discharges.[8]

LH waves drive current by transferring momentum and energy from the wave to electrons traveling along the magnetic field with velocities near the parallel phase velocity of the wave $v_\parallel$ through Landau damping, creating an asymmetric plasma resistivity. The resulting current drive efficiency is inversely proportional to the plasma electron density n_e and the square of the parallel refractive index, $n_\parallel \equiv ck_\parallel/\omega$.[4,9]

Wave accessibility and parametric decay instabilities[5,10] (PDI) have been suggested as possible explanations for the density limits observed on previous LHCD experiments. Considering only the accessibility criterion,[11,12] any wave for which $n_\parallel$ is greater than $n_{\parallel,\mathrm{crit}}$ will be able to penetrate to the core of the plasma, provided that the wave is not fully absorbed in the edge region first. Here,

$$n_{\parallel \mathrm{crit}} \approx \sqrt{1 - \frac{\omega_{pi}^2}{\omega^2} + \frac{\omega_{pe}^2}{\omega_{ce}^2}} + \frac{\omega_{pe}}{|\omega_{ce}|}. \tag{1}$$

LH (slow) waves for which the launched $n_\parallel$ is locally less than the critical value given by Eq. (1) anywhere in the plasma will be mode converted to the fast wave at the point where $n_\parallel = n_{\parallel \mathrm{crit}}$ and reflected back to the plasma edge. It is important to note that this discussion of wave accessibility ignores possible changes to $n_\parallel$ that can occur along the ray path. This effect is taken into account in the simulations that are discussed later in this paper.

PDI[13,14] is a three wave coupling process by which an incident lower hybrid wave at a frequency $\omega = \omega_0$ decays into a low frequency branch, at $\omega = \omega_1 \sim \omega_{ci} \ll \omega_0$, and a daughter LH wave, at $\omega = \omega_0 - \omega_1$. The wavenumber of the daughter LH wave may upshift substantially, thereby reducing the current drive efficiency. If the upshift of $n_\parallel$ is severe enough, the daughter wave may damp on ions as well. Results from the Alcator C tokamak[15] indicate a density limit for efficient current drive at $\omega_0/\omega_{LH} \sim 2$.[5] Here

$$\omega_{LH}^2 \approx \frac{\omega_{pi}^2}{1 + \omega_{pe}^2/\omega_{ce}^2} \tag{2}$$

is the lower hybrid frequency. Because ω_{LH} increases with magnetic field and density, parametric decay is of particular importance on high density, high field experiments such as Alcator C.

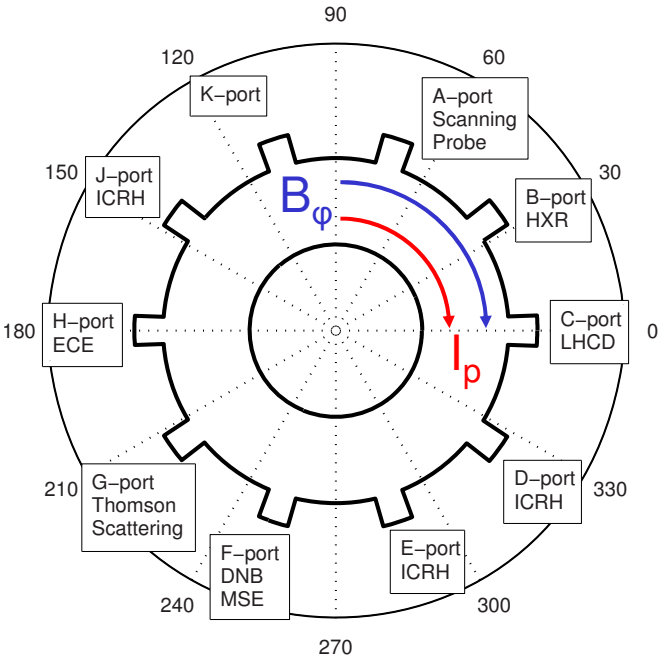

FIG. 1. (Color online) Location of the C-Mod LHCD launcher (at C-port), HXR camera (at B-port), and selected heating and diagnostic systems. Lower hybrid waves are primarily launched from C-port toward B-port in current drive operation. The direction of both the plasma current and toroidal magnetic field are clockwise when viewed from above.

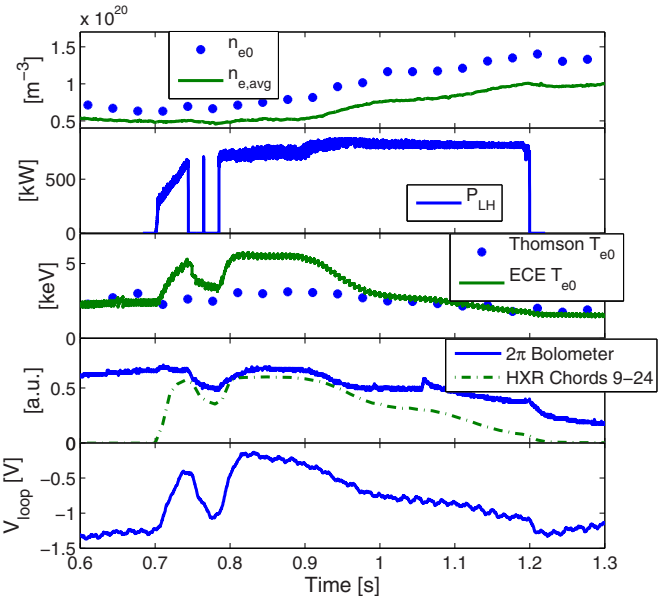

FIG. 2. (Color online) Time evolution of several key plasma parameters during a ramped density L-mode discharge with high power LHCD. Disagreement between the Thomson scattering and ECE temperature measurements from 0.7 to 1 s is due to nonthermal ECE emission. Shot number =1080429017.

The propagation and absorption of LH waves is treated in this paper by use of the ray tracing and Fokker–Planck codes GENRAY (Ref. 16) and CQL3D.[17] The GENRAY ray tracing package makes use of the Wentzel–Kramers–Brillouin (WKB) and geometrical optics approximations to represent waves as packets of photon energy traversing through the plasma. A series of rays are launched to approximate the wave-number spectrum produced by a three-dimensional antenna structure. Each ray is independently followed through the plasma until it reaches a damping threshold, at which point the ray is terminated. The effects of wave accessibility, including variation of $n_{\|}$ along the ray, are included in the code. The output of GENRAY is passed to the bounce-averaged Fokker–Planck solver CQL3D to calculate the perturbed electron distribution function. The perturbed distribution function calculated by CQL3D is then used to recalculate the wave damping in GENRAY, and this process is iterated until the result converges.

II. EXPERIMENTAL RESULTS

The LHCD antenna on Alcator C-Mod consists of a 4 row by 22 column waveguide phased array operating at a frequency of 4.6 GHz.[1] By varying the relative phase between adjacent waveguides, the peak of the launched $n_{\|}$ spectrum can be varied from ~1 to 4 in both the current drive and countercurrent drive directions. A 32-chord poloidally viewing Hard X-Ray (HXR) diagnostic on C-Mod (Ref. 18) is used both for localizing the fast electron bremsstrahlung emission and for comparing the relative magnitude of the x-ray count rate between discharges. The HXR count rate can also be taken as a proxy for the density of the fast electron tail generated by LHCD, although they are not directly proportional. The locations of the LHCD launcher and HXR camera relative to other systems on the tokamak are shown in Fig. 1.

By observing the decrease in HXR emission as the plasma density was increased, it was determined that LH waves are not absorbed in the core of C-Mod L-mode plasmas at line averaged densities above $\bar{n}_e \sim 1 \times 10^{20}$ m^{-3}. Additionally, electric currents and electron density in the scrape off layer (SOL) increase during LHCD above this same density threshold. These observations suggest a shift of wave absorption from inside the separatrix into the SOL at high density.

Unless otherwise noted, the data presented in this paper are from Ohmic L-mode discharges in deuterium at typical C-Mod parameters (B_ϕ=5.4–7 T, I_p=0.8–1.1 MA). In order to cover the largest number of experimental conditions with the number of discharges available, the plasma density was ramped throughout each discharge. Figure 2 shows the time evolution of several key plasma parameters during a typical ramped L-mode discharge. Ramps up and down in density were performed to verify that there was no hysteresis in the density scans.

A. Hard x-ray bremsstrahlung

Since the thermalization rate of the fast electrons due to collisions is proportional to plasma density, it follows that, for a fixed source of fast electrons in an otherwise uniform plasma, the fast electron population should be inversely proportional to plasma density. A scaling of current drive efficiency proportional to $1/n_e$ is predicted based on the increase of collisionality with density.[4] This scaling is confirmed by simulations which will be discussed later in this

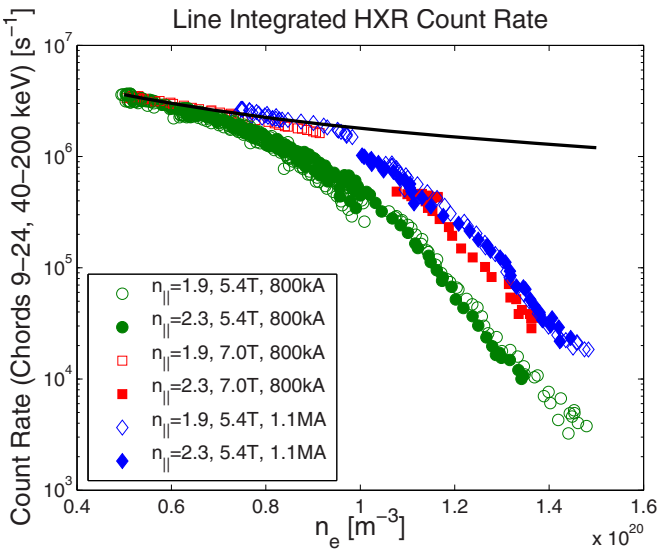

FIG. 3. (Color online) Line integrated x-ray emission on the central chords as a function of line averaged density. Data are plotted on a semilogarithmic scale for x-rays between 40 and 200 keV. The black curve represents a $1/n_e$ falloff. The count rates in this figure are normalized to the square root of net LH power.

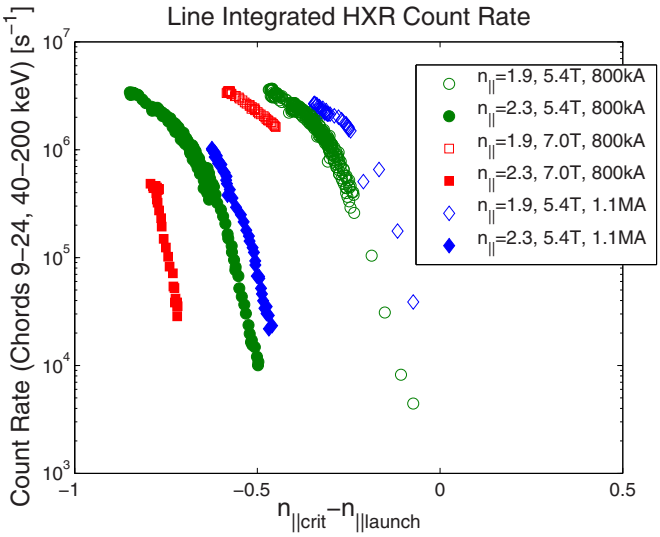

FIG. 4. (Color online) Fast electron bremsstrahlung emission as a function of $n_{\|\mathrm{crit}}-n_{\|\mathrm{launch}}$. The value of $n_{\|\mathrm{crit}}$ is evaluated using line averaged density and on-axis magnetic field.

paper. Figure 3 shows that the experimental HXR count rates fall much more steeply than the expected $1/n_e$ above $\bar{n}_e \sim 0.9\times10^{20}$ m^{-3}.[8] This is particularly true for the 5.4 T, 800 kA case, which deviates from the $1/n_e$ curve starting near $\bar{n}_e=7\times10^{19}$ m^{-3}. The HXR count rates at higher magnetic field and plasma current drop more slowly as density rises, but are still two orders of magnitude lower than the $1/n_e$ prediction at $\bar{n}_e=1.5\times10^{20}$ m^{-3}.

The count rates shown in Fig. 3 have been normalized to the magnitude of the wave electric field (square root of net LH power). The data represent a range of net LH power from 550 to 900 kW. The square root of LH power scaling is used here as it leads to the tightest grouping of the experimental data.

Although a violation of the accessibility criterion above 1×10^{20} m^{-3} may appear to explain the results of Fig. 3, there are several points which contradict the accessibility criterion explanation. First, the data taken at $n_\|=2.3$ (closed symbols) and the data taken at $n_\|=1.9$ (open symbols) do not show a significant difference in count rate as the density changes. If the loss of core bremsstrahlung emission was related to the accessibility criterion, one would expect the lower value of $n_\|$ to be affected more severely and at a lower density than the higher value of $n_\|$. The two sets of data are nearly coincident across a range of density, magnetic field, and plasma current. In addition, the accessibility criterion is satisfied at both $n_\|$ of 1.9 and 2.3, even for the highest density shown in Fig. 3 at the lowest magnetic field. Figure 4 shows the bremsstrahlung emissivity as a function of $n_{\|\mathrm{crit}}-n_{\|\mathrm{launch}}$. The value of $n_{\|\mathrm{crit}}$ is evaluated based on the line averaged density and on axis magnetic field. According to results from FTU,[19] accessibility should only be an issue for $n_{\|\mathrm{crit}}-n_{\|\mathrm{launch}}>0.05$ when calculated in this manner.

The density limit observed on Alcator C has been attributed to PDI as $\omega\rightarrow2\omega_{\mathrm{LH}}$.[5–10,13,14] LHCD efficiencies proportional to $1/\bar{n}_e$ with strong nonthermal electron cyclotron emission (ECE) and HXR emission were observed on Alcator C up to $\bar{n}_e=10^{20}$ m^{-3}.[20] The Alcator C results were obtained at high toroidal field ($B_\phi\sim8-10$ T) in hydrogen plasmas such that $\omega/\omega_{\mathrm{LH}}\sim2$ at $\bar{n}_e=10^{20}$ m^{-3}. The bremsstrahlung data from C-Mod show a precipitous drop in emission below $\omega/\omega_{\mathrm{LH}}\sim3.75$, as can be seen from Fig. 5. All of the data from C-Mod occur at values of $\omega/\omega_{\mathrm{LH}}$ in excess of 3, for which there should be no significant parametric decay according to earlier results. The discrepancies between the data at 5.4 and 7.0 T show that although the experimental bremsstrahlung emission scales as a function of $\omega/\omega_{\mathrm{LH}}$ at a given value of magnetic field, comparisons between different values of magnetic field at a fixed density do not agree with the $\omega/\omega_{\mathrm{LH}}$ scaling. An increase in magnetic field will

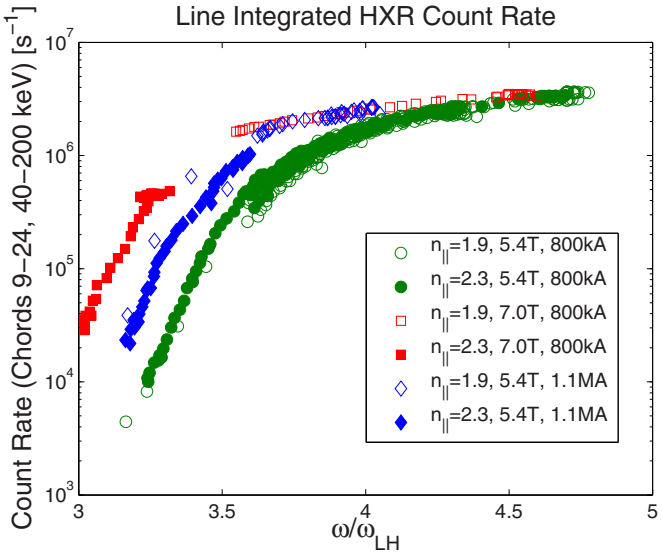

FIG. 5. (Color online) Fast electron bremsstrahlung as a function of $\omega/\omega_{\mathrm{LH}}$ at $B_T=5.4$ and 7.0 T. ω_{LH} is computed using line averaged electron density and on axis magnetic field.

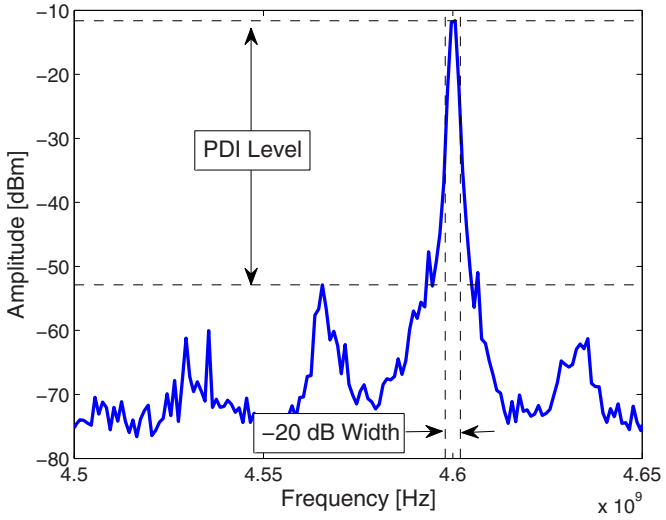

FIG. 6. (Color online) Frequency spectrum measured by a spectrum analyzer connected to an RF probe located on the midplane at C-port. The "PDI level" and "−20 dB width" are shown schematically.

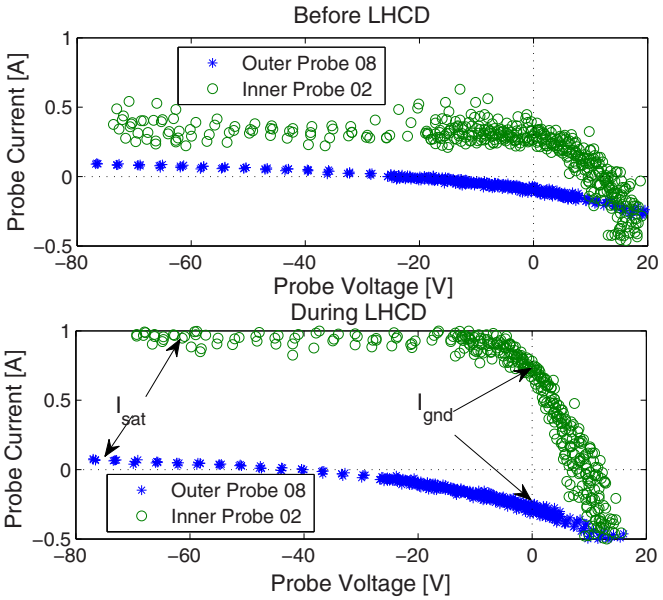

FIG. 7. (Color online) *I-V* characteristic for Langmuir probes mounted in the inner and outer lower divertors before and during high power LHCD. The ground current I_{gnd} and the ion saturation current I_{sat} are shown. Both probes are located at $\rho \sim 0.008$ m. Shot number=1080402031.

increase the value of ω_{LH}, but the data show an increase in HXR emission at a fixed density for the higher field. The discrepancy seen in Fig. 5 between the 5.4 and 7.0 T data shows that bremsstrahlung emission is a function of density, not ω/ω_{LH}. This indicates that ω/ω_{LH} is not the critical parameter for the density limit observed on C-Mod.

The microwave spectrum in the vicinity of the pump frequency was recorded for several of the discharges shown in Fig. 5 by measuring the microwave frequency spectrum picked up by a probe mounted between two rows of the LH launcher. The PDI level is defined here as the amplitude of the pump wave minus the amplitude of the strongest downshifted sideband measured in decibels, as shown schematically in Fig. 6. This gives a relative measure of the strength of the parametric decay instabilities. Although the PDI level rises with line averaged density, at the highest densities (and consequently lowest values of ω/ω_{LH}), the strongest sideband is at least −20 dB relative to the pump, corresponding to less than 1% of the total power.

It is important to note that the measurement location for PDI is in close proximity to the LH launcher and the relative magnitude of the downshifted sideband may be higher away from the launcher. However, we have observed PDI levels as high as −10 dB relative to the pump wave in the same location on C-Mod at higher density ($\bar{n}_e > 2\times10^{20}$ m^{-3}),[21] where strong PDI would be expected. Therefore, we consider this to be a reliable measurement.

Experiments on the FTU LHCD experiment[6] indicate that parametric decay can contribute to a loss of LHCD efficiency under conditions of high density and low temperature in the SOL. The PDI signature in the FTU experiment is seen through broadening of the pump wave as opposed to discrete downshifted harmonics of the ion cyclotron frequency seen on C-Mod. On C-Mod we see extremely small increases in pump width as density rises (less than 25% increase in width at −20 dB and no observable change at −10 dB between 5×10^{19} and 1.5×10^{20} m^{-3}), which is inconsistent with the severe spectral broadening needed to explain the observed density limit.

B. Scrape-off-layer currents

Langmuir probes mounted in the upper and lower divertor regions of C-Mod are typically operated in a swept *I-V* configuration for measurement of electron density and temperature. As the potential difference between the probe and the vacuum vessel wall passes through zero, the "ground current" collected by the probe, I_{gnd}, can be measured. This current is equal to the free flowing current into the wall parallel to the magnetic field. Figure 7 shows the point on the *I-V* characteristic where I_{gnd} is measured for two probes before and during a high power LHCD pulse. The convention taken here is that a positive current will be measured if the probe is collecting ions. Since the geometry of the probe is known, the parallel current density incident on the probe can be determined from the current collected by the probe based on the angle of incidence of the field line and the radius of the probe electrode. Figure 8 shows the location of the C-Mod divertor Langmuir probes.

In normal operation, the parallel electric current in the SOL, $J_{\|}$, measured by the divertor probes is less than $\sim1\times10^5$ A/m^2 and of similar magnitude on all of the probes. During high power LH operation at line averaged densities above $\sim1\times10^{20}$ m^{-3}, the magnitude of $J_{\|}$ measured by some probes increases dramatically. In upper null discharges, the current flows between the inner and outer sections of the upper divertor. The polarity difference between the inner and outer divertors indicates that the current is leaving the upper inner divertor, traveling around the bottom of the plasma, and returning to the vacuum vessel wall on the upper outer divertor in upper single null (USN). When

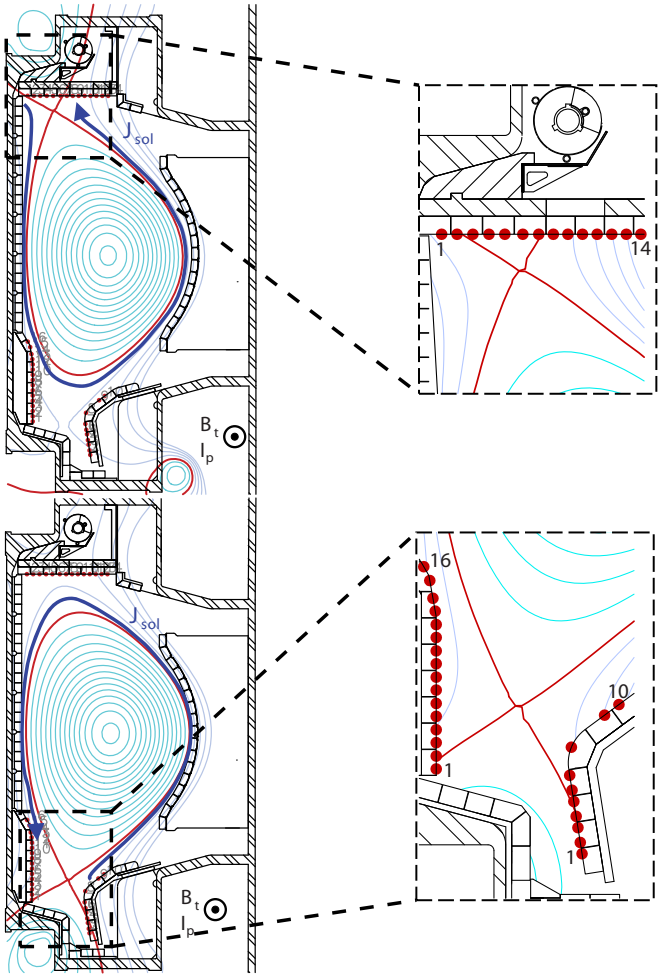

FIG. 8. (Color online) Direction of the SOL currents projected on the poloidal cross section for USN and LSN. In both configurations the SOL current flows in the same toroidal direction as B_ϕ and I_p. The detailed insets show the location of the upper and lower probes relative to the separatrix in upper null and lower null, respectively. Probes are numbered sequentially for the inner, outer, and upper divertors.

projected in the toroidal direction, this corresponds to the same direction as the current in the confined plasma, I_p, if we assume that the SOL current is traveling parallel to the magnetic field. In the lower single null (LSN) configuration, the current leaves the lower outer divertor and flows toward the lower inner divertor. Near double null, the currents sometimes flow from the lower outer divertor to the upper outer divertor. Figure 9 shows the waveforms of the SOL currents in an USN discharge near double null. The two probes, which lie on approximately the same flux surface, measure values of I_{gnd} which are nearly equal in magnitude but opposite in polarity. Again, this is the same direction as I_p. Figure 8 shows the direction of the SOL currents as projected onto the poloidal cross section for both upper and lower null configurations. The direction of the SOL currents does not change when the launched $n_\parallel$ direction is reversed, suggesting that a Landau interaction between the LH waves and the SOL plasma is not responsible for the currents.

Figure 10 shows the SOL current density for the USN discharges in Fig. 3 as a function of line averaged density. The SOL currents suddenly increase in magnitude at

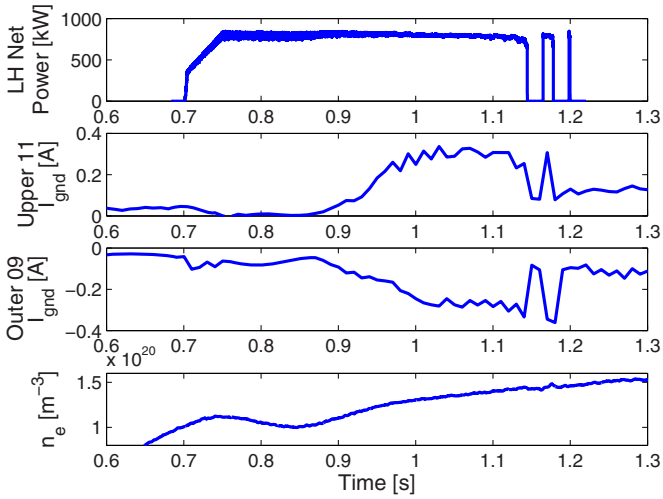

FIG. 9. (Color online) Waveform of SOL currents observed during LHCD experiments at high density in upper single null (near double null). Modulation of the SOL currents with LHCD power is evident during trips at the end of the LH pulse. The largest SOL currents connect between probe 11 in the upper divertor and probe 9 in the lower outer divertor for this discharge. For this discharge $\rho_{\text{launch}} \sim 0.025$ m and $\rho_{\text{probe}} \sim 0.015$ m. Shot number =1080513019.

$\bar{n}_e \sim 1.0 \times 10^{20}$ m^{-3}, the same density at which fast electron bremsstrahlung disappears from the central HXR chords. Enhanced SOL currents during high power LHCD have been observed in LSN as well. This suggests that at high density the LH waves are absorbed in the SOL rather than inside the separatrix.

Collisionally damped lower hybrid waves have been observed to drive current on open field lines where $k_\parallel v_t/\omega \ll 1$ in the linear H-1 device.[22] An upper limit on the driven current can be obtained by assuming that $E_\parallel(z)$ is a constant. This assumption reduces Eq. 3 of Ref. 22 to

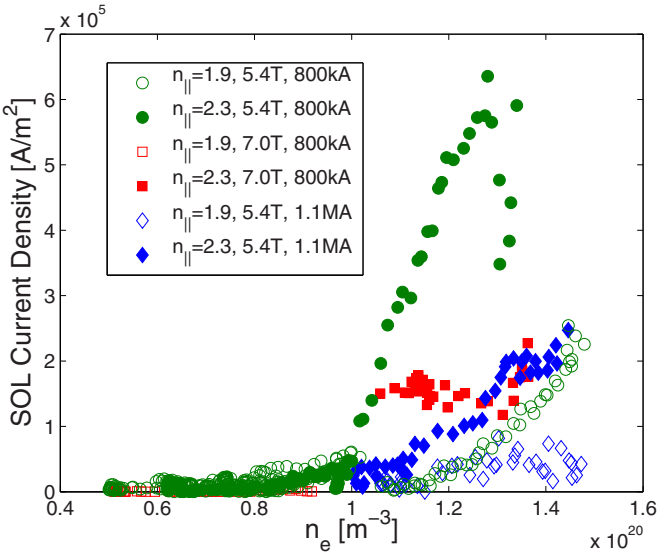

FIG. 10. (Color online) Peak SOL current density as a function of line averaged density in USN L-mode discharges, as measured by the outer upper divertor Langmuir probes. Data at $n_\parallel = 2.3$ show significantly more current than data at $n_\parallel = 1.9$. SOL currents are strongest for smaller values of magnetic field and plasma current.

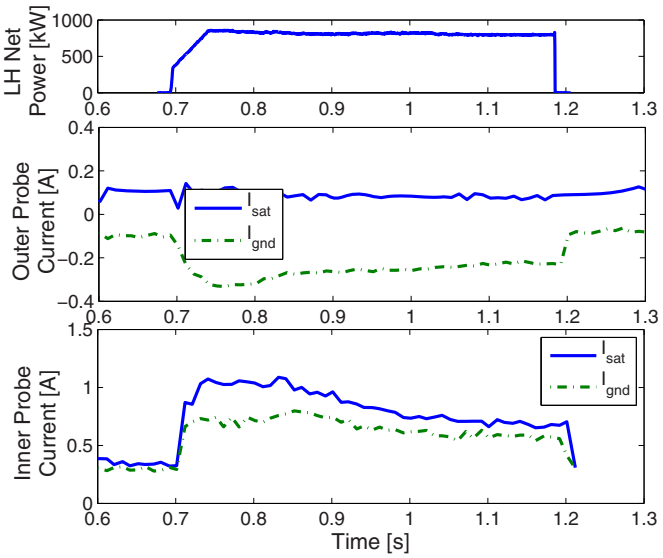

FIG. 11. (Color online) Comparison of I_{gnd} and I_{sat} on divertor probes in LSN configuration. I_{gnd} on the inner divertor is near the limit set by I_{sat}, while on the outer divertor $|I_{gnd}|$ exceeds $|I_{sat}|$. Shot number=1080402031.

$$\langle j_{\parallel} \rangle = -4.5978 \times 10^{-11} \frac{q}{m_e} \frac{\omega_{pe}^2}{\omega^3} k_{\parallel} |E_{\parallel}|^2. \quad (3)$$

The wave electric fields in the SOL of C-Mod are estimated to be ~10 kV/m for a net LH power of 900 kW. At a density of 1×10^{19} m^{-3}, a parallel current density of 236 A/m^2 would result. Even if the estimates of the wave electric fields in the SOL are too low by a factor of 10, the observed current is still far too large to be explained by direct current drive via collisional absorption of the LH waves.

Figure 11 shows the values of ion saturation current, I_{sat} and I_{gnd}, for probes on the inner and outer divertor surfaces in a lower single null discharge. On the ion-collecting end of the flux tube (which in LSN is the inner divertor), there is a substantial increase in I_{sat} during LHCD. Interestingly, there is no corresponding change in I_{sat} at the electron collecting end of the flux tube (which in LSN is the outer divertor). On the end of the field line which collects ions, $|I_{gnd}|$ cannot exceed $|I_{sat}|$, and the ratio $|I_{gnd}/I_{sat}|$ is near 0.8 with and without LHCD. On the end of the field line collecting electrons, $|I_{gnd}|$ would be limited by the electron saturation current. However, the electron saturation current is larger in magnitude than $|I_{sat}|$ by roughly the ratio of the deuteron mass to the electron mass. Consequently $|I_{gnd}|$ may easily exceed $|I_{sat}|$ on the electron collecting end of the field line.

The increase in the SOL current appears to be due to an increase in density, and thus I_{sat}, at the ion-collecting end of the field line. The increase in I_{sat} then allows the SOL current (which cannot exceed I_{sat} at the ion-collecting end of the flux tube) to increase as well. The driving mechanism of the SOL current is consistent with a thermoelectric current[23,24] flowing from the hotter, less dense electron collecting divertor plate to the colder, denser ion-collecting divertor plate. The temperature and density asymmetry on the ion and electron collecting divertors can be inferred from the shapes of the *I-V* curves in Fig. 7.

We hypothesize that the increase of plasma density at the ion-collecting divertor plate may be caused by a transition from a partially detached divertor regime to a sheath-limited or high-recycling divertor regime.[25] The change in divertor behavior is likely caused by an additional source of power in the detached region (i.e., parasitic absorption of LHCD in the SOL as supported by the modeling in this section). LH waves absorbed in the SOL may also contribute to an increase in ionization rate for neutrals in the divertor region. The change in recycling conditions and increase in ionization would lead to higher ion saturation current on the ion-collecting end of the field line, which then supports a higher thermoelectric SOL current.

10 eV is a typical temperature for the region of the SOL where the enhanced currents are observed during LHCD. At this temperature the resistivity of the SOL plasma is 6.5×10^{-5} Ω m. Joule's law can be used to estimate the resistive power dissipated in the SOL. If we take the current to be evenly distributed in a 1 cm thick annulus surrounding the separatrix (based on the characteristic radial width of the SOL currents observed on the divertor Langmuir probes), this results in a dissipated resistive heating power of approximately 850 kW, which is similar in magnitude to the total injected LH power in these discharges. This suggests that a large fraction of the injected LH power may be transferred into supporting the SOL currents. The estimated total current in the SOL during LHCD is ~20 kA, again assuming that the current is evenly distributed in a 1 cm thick annulus surrounding the separatrix.

III. SIMULATION OF WAVE BEHAVIOR

The discharges discussed in Sec. II have been modeled with the ray tracing/Fokker–Planck package GENRAY/CQL3D to determine if the experimentally observed reduction in the core fast electron bremsstrahlung would be predicted based on conventional modeling techniques. The GENRAY/CQL3D code package includes a fast electron bremsstrahlung x-ray synthetic diagnostic that can be directly compared with the experimental HXR results in Sec. II A. Figure 12 shows the measured and simulated bremsstrahlung emission for a range of plasma parameters. The simulated HXR emission is calculated based on a net LH power of ~800 kW, which was the power level used in the normalization of the experimental results shown in Fig. 3. The simulations use experimental profiles of plasma density and temperature, along with experimental values of toroidal electric field and Z_{eff} from the same discharges plotted in the experimental HXR data. Although the cutoff for LH waves is located outside the separatrix in the experiment, an artificial cutoff is imposed just inside the separatrix in the conventional version of this model.

The simulated emission at values of $\bar{n}_e$ between 5×10^{19} and 1×10^{20} m^{-3} is higher than the experimental data by a factor of ~5, while at 1.5×10^{20} m^{-3} the discrepancy is two to three orders of magnitude. However, the simulated emissivity is in qualitative agreement with the $1/n_e$ estimate. As with the experimental data, the simulations predict nearly identical emissivity for $n_{\parallel}$ values of 1.9 and 2.3.

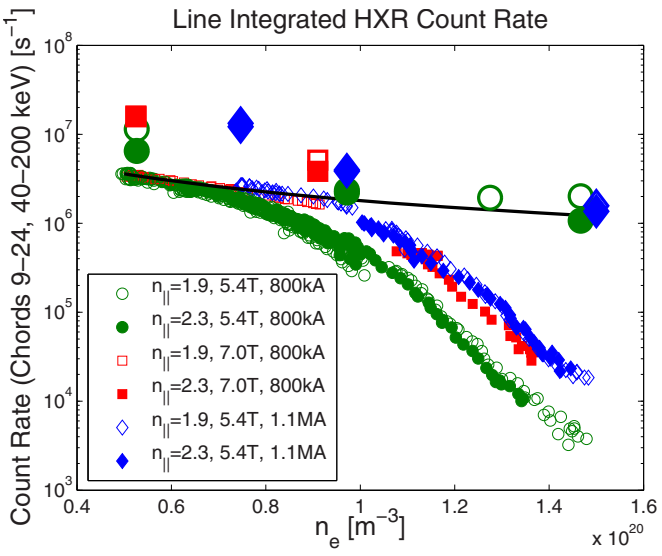

FIG. 12. (Color online) Simulated and measured HXR emission as a function of line averaged density. The output of the synthetic diagnostic is shown with large symbols, while the experimental data are shown with small symbols. Simulations are based on 800 kW of net LH power.

Figure 13 shows the simulated ray trajectories for a 5.4 T, 800 kA plasma at $\bar{n}_e = 1.4 \times 10^{20}$ m^{-3}. The simulated ray trajectories in high density ($\bar{n}_e \geq 1 \times 10^{20}$ m^{-3}) discharges show that some of the rays are trapped in the edge region of the plasma immediately after launch due to marginal wave accessibility. These "trapped" rays reflect between the cutoff at the plasma edge and the high density mode conversion layer until $n_{||}$ upshifts sufficiently for penetration into the core.

GENRAY has been used to investigate the strength of

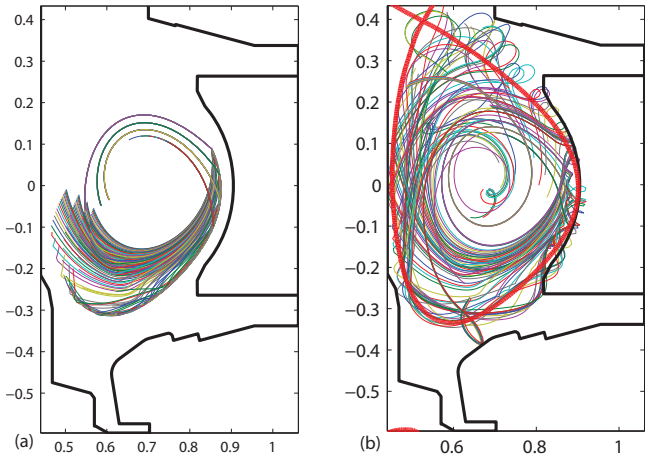

FIG. 13. (Color online) (a) GENRAY simulation showing rays trapped near the edge of the plasma. Each ray corresponds to a specific launch location and launched value of $n_{||}$. The highest $n_{||}$ rays penetrate to near the core of the plasma, while the lower $n_{||}$ rays stay close to the edge. Rays propagating in the current drive direction move downward from the low field side (LFS) launch point, while rays propagating in the countercurrent drive direction move upward from the LFS launch point. The cutoff layer in this simulation is located at the separatrix and the vacuum vessel walls are superimposed for reference. The rays are truncated for clarity after a fixed distance. (b) Ray trajectories including a 2D SOL model and reflections from the vacuum vessel. The separatrix location is indicated by a bold line. $\sigma_T(\theta)$ is estimated on the basis of flux expansion.

single-pass damping for the simulated discharges. Stopping all rays immediately after a single radial transit (i.e., one pass from the antenna into the plasma and out to the separatrix) decreases the simulated HXR emission by four orders of magnitude at 1.5×10^{20} m^{-3}, and by more than two orders of magnitude at 5×10^{19} m^{-3}. This shows that single-pass damping is weak in these relatively cold discharges, even at the low density end of the scan. We must properly account for what happens to the rays as they reflect from, or are absorbed at, the edge of the plasma. For the synthetic diagnostic HXR emissivity to agree fully with the experimental data, some amount of reflection from the cutoff must be taken into account, but there also must be some loss mechanism at the edge.

A. Scrape-off-layer model for GENRAY

A close examination of the ray trajectories in Fig. 13 shows that a more careful treatment of the pedestal and SOL regions is necessary to represent the wave behavior in the edge region accurately. Artificially imposing a cutoff at the separatrix creates a narrow region where rays may become trapped between the low density cutoff layer and the high density mode conversion layer. To account for this, a SOL model has been added to GENRAY. Magnetic fields in the SOL are imported directly from a magnetic field equilibrium reconstruction. The SOL is only included in the GENRAY code and is not a part of CQL3D. Consequently, quasilinear wave absorption is not calculated in the SOL, and the radiation from fast electrons born in the SOL is not included in the synthetic diagnostic.

GENRAY includes collisional damping effects both inside the separatrix, where collisional damping is small relative to Landau damping, and in the SOL. At the low temperatures encountered in the SOL, collisional damping can be comparable to or exceed Landau damping for low $n_{||}$ waves. Information regarding the absorption of the rays in the SOL is not directly included in the quasilinear diffusion coefficient used in CQL3D, although the power in the ray is reduced appropriately after passing through the SOL. The effects of collisional damping in the SOL will be discussed further in Sec. III B

A two-dimensional (2D) SOL profile, for which the density scale length σ_n is a function of poloidal angle, has been implemented in GENRAY. The 2D SOL model also includes the C-Mod vacuum vessel and limiter geometry and reflects rays that intersect the metallic surfaces. Figure 13 shows the ray trajectories for a high density ($\bar{n}_e \sim 1.5 \times 10^{20}$) discharge with the 2D SOL model. Although shifts of $k_{||}$ that occur in the SOL reduce the predicted x-ray emissivity, the experimental data are still several orders of magnitude below that predicted by CQL3D. Therefore, there must be an additional mechanism or mechanisms responsible for the discrepancy.

B. Collisional absorption in the SOL

The simulations previously discussed do not include any contribution of damping in the SOL calculated by GENRAY. The collisional absorption of the LH waves can be strong in regions of high density and low temperature

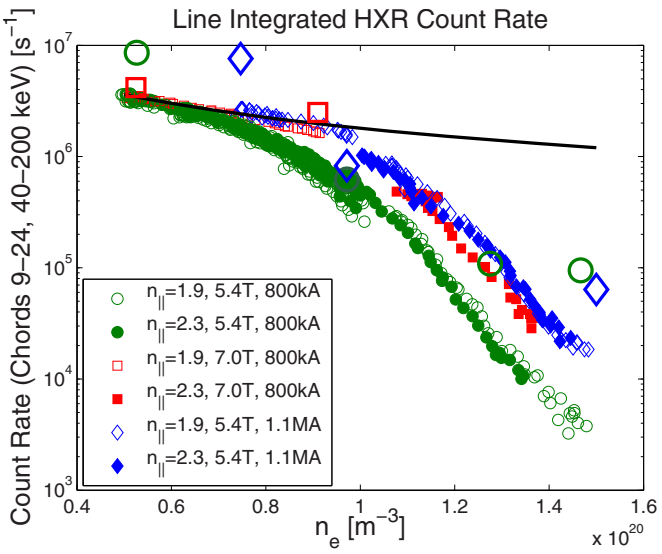

FIG. 14. (Color online) Fast electron bremsstrahlung emission predicted by GENRAY/CQL3D code package with a two-dimensional SOL model including the effects of collisional damping in the SOL. The large symbols are simulation results, while the small symbols are experimental data.

($T_e < \sim 10$ eV). At temperatures above ~ 10 eV, the damping is small even at high density. Collisional damping is estimated following the approach in Ref. 26, where the electron mass m_e is replaced with $m_e(1+i\nu_{ei}/\omega)$ in the cold plasma dispersion relation, where ν_{ei} is the effective electron-ion momentum collision frequency.

By including the effect of power absorbed in the SOL due to collisional damping, the x-ray emissivity at high density is reduced significantly.[27] (See Fig. 14.) The agreement between experimental data and predictions from CQL3D is improved across the entire density range, most notably at 1.5×10^{20} m^{-3}, where the discrepancy was reduced from a factor of $\sim$100–1000 to a factor of $\sim$3–30.

It should be noted that the assumed SOL parameters are identical for all of the simulation data points in Fig. 14. The modeled temperature in the SOL decays exponentially with an e-folding length σ_T of 0.005 m until the temperature reaches a minimum of 5 eV, beyond which the plasma temperature remains constant. These values are consistent with measurements of the SOL temperature profiles typically observed in C-Mod L-mode discharges. The density e-folding length varies between 0.1 m in the divertor regions and 0.02 m on the outer midplane. These values are typical for L-mode discharges but are not exact representations of profiles in the discharges being modeled.

Collisional absorption in the SOL is sensitive to the specifics of both the temperature and density profiles. Since the absorption peaks in areas of low temperature and high density, such as divertor regions, the exact path of the ray will determine the level of damping in the SOL. At a fixed density, the experimental x-ray emissivity is consistently weaker for the 5.4 T, 800 kA discharges with $\bar{n}_e$ above $\sim 8\times10^{20}$ m^{-3}; however, the simulation data do not show this same trend. This may be due to the sensitivity of the SOL absorption to the temperature and density profiles. Results from Alcator C (Ref. 20) show an increase in current drive efficiency at higher magnetic field. The increase in efficiency was attributed to an increase in electron temperature at higher field. There may well be small differences in the SOL profiles as a function of plasma current and magnetic field, although in the discharges considered there are no profile measurements in the SOL. Still, the strong downward trend in x-ray emission as density increases suggests that a damping mechanism in the SOL that increases with n_e and decreases with T_e may be largely responsible for the absence of fast electrons in the plasma.

Although collisional absorption does not by itself lead to a net driven current in the plasma, it is possible that the SOL currents discussed in this section may be due to asymmetric heating in the SOL. If the waves leaving the LH launcher deposit their energy preferentially in one direction along the field lines, this can cause a parallel thermal gradient, which in turn can drive a thermoelectric current along open field lines.[24] However, there is some inconsistency in this explanation. If a thermal gradient is responsible for driving the currents in the SOL, then the region of plasma where the waves are absorbed through collisional damping would heat up. The collisional damping rate falls sharply as plasma temperature rises above ~ 10 eV. Furthermore, measurements of T_e in the divertors do not show a change in temperature on either end of the field line during the application of LHCD.

This same reasoning suggests that it may be possible to "burn through" the observed density limit. If sufficient energy is deposited in the SOL, the temperature will rise and the collisional damping rate will fall, thereby increasing the amount of power absorbed on closed flux surfaces. This self-regulating mechanism could provide a means to ameliorate the density limit phenomenon, although if this is possible the critical power threshold is above 900 kW on C-Mod.

Another possible solution to the problem of LH wave absorption in the SOL may be to increase the temperature inside the separatrix through ion cyclotron resonance heating (ICRH), such that waves with reduced penetration to the core plasma are still absorbed before refracting back into the SOL. If the single-pass absorption is high for all rays, then the loss in the SOL may be significantly reduced. Alternatively, dramatically increasing $n_{||}$ while keeping the plasma temperature constant will increase single-pass absorption at the cost of overall current drive efficiency.

LHCD experiments at high density on FTU show an increase in fast electron bremsstrahlung following the application of lithium to the plasma facing components.[6] This has the effect of both decreasing density and increasing temperature in the edge of the plasma. Although the proposed explanation for reduced bremsstrahlung at high density on FTU (spectral broadening of the LH waves due to parametric decay instabilities) differs with that of C-Mod, both explanations point toward using higher edge temperature and lower edge density as a means to reduce parasitic losses in the edge.

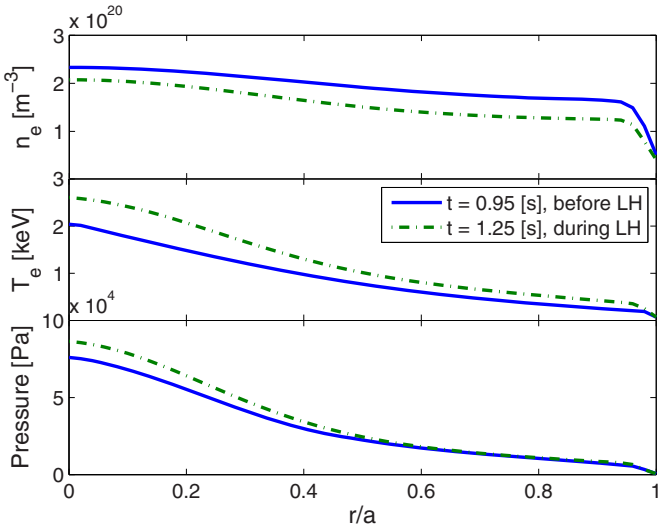

FIG. 15. (Color online) Changes in H-mode density, temperature, and pressure profiles with the application of LHCD. Shot number=1080306013.

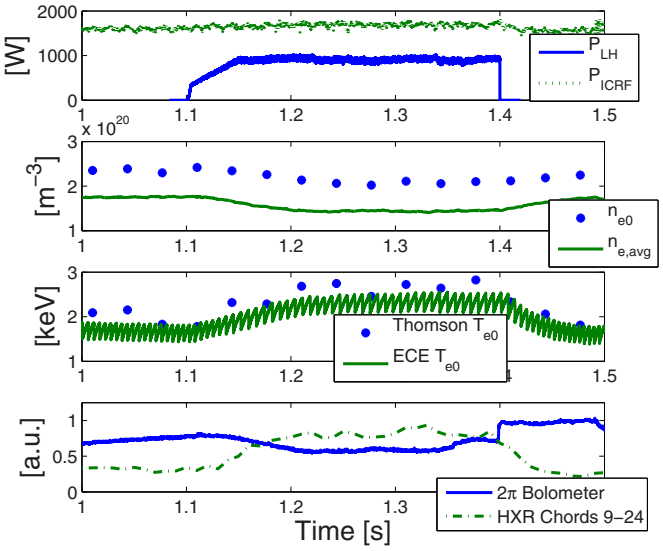

FIG. 16. (Color online) Low density H-mode with LH induced pedestal modification. T_e and HXR emission increase during the application of LHCD while n_e, V_{loop}, and radiated power decrease. Shot number =1080306013.

IV. IMPLICATIONS FOR LHCD IN H-MODE ON ALCATOR C-MOD

In general, H-mode discharges have considerably higher line averaged densities than L-modes. On C-Mod, H-modes with $\bar{n}_e < 1.5\times10^{20}$ are extremely difficult to obtain, and the highest performance H-modes have $\bar{n}_e > 2.0\times10^{20}$. Given that the density of H-mode discharges is above the L-mode density limit for LHCD, the scaling of the LHCD density limit in H-mode is of considerable interest for the future application of LH current profile control on C-Mod.

When LHCD is applied to relatively low density, $\bar{n}_e < 2\times10^{20}$ m^{-3}, low Z_{eff}, ICRH heated, H-mode plasmas on C-Mod, substantial changes occur in the plasma despite the fact that the density is above the limit described in Sec. II. During the application of high power LHCD, the density profile relaxes, with a decrease in density at the top of the pedestal and an increase in density at the foot.[28] The temperature simultaneously increases at the top of the pedestal but remains nearly constant at the pedestal foot. These complementary changes in the temperature and density result in a nearly unchanged pedestal pressure profile, while the pressure at $r/a < 0.6$ increases by 10%–15%. The temperature, density, and pressure profiles for an H-mode discharge before and during LHCD are shown in Fig. 15.

The changes to the pedestal become more prominent as P_{NET}, the total heating power (ICRH, LHCD, and Ohmic) minus the radiated power increases. Since the radiated power increases with Z_{eff}, this effect has only been seen in clean discharges immediately following a thorough boronization.[29] Although P_{NET} includes the sum of all heating power, it should be noted that these pedestal changes have not been observed without a combination of both ICRF and LHCD. Figure 16 shows the changes in several key plasma parameters during an H-mode discharge that has a strong modification to the pedestal. Both the core and line averaged density decrease during the application of LHCD, but the core temperature increases. Radiation from the plasma measured by the 2π bolometer[30] also decreases when the LHCD is turned on, indicating increased impurity transport. Although the HXR camera shows a considerable background count rate during the ICRF only portion of the H-mode, a clear increase can be seen during LHCD.

The change to the H-mode density pedestal induced by LHCD increases density in the SOL. This moves the cutoff layer further from the separatrix where T_e is lower and collisional damping is stronger. However, the lower core density causes refraction to be less severe, allowing rays to more directly access the hot core of the plasma. Also, the temperature in the core plasma, and therefore wave damping inside the separatrix, increases. The net result of these competing effects is not immediately apparent and must be addressed by examining the experimental data and comparing with models of the H-mode discharge in its unperturbed state (immediately prior to the application of LHCD) and in its perturbed state.

Figure 17 shows the HXR emission during several H-mode discharges modified by ~900 kW of LHCD. The black points represent the H-mode discharges, all of which had a launched $n_{\parallel}$ of 2.3. The bremsstrahlung emission during these discharges was significantly higher than for the high density L-modes at comparable line averaged density. The background HXR level due to ICRF is subtracted from the H-mode data in Fig. 17.

The current driven in an H-mode discharge with LHCD can be estimated based on the change in loop voltage because the plasma remains in a stationary state for a sufficient time for the current to redistribute. To estimate the amount of current driven, it is necessary to consider not just the ratio of loop voltage prior to and during LHCD, $V_l(t_2)/V_l(t_1)$, but also the change in resistivity due to temperature,

$$\frac{\eta(t_2)}{\eta(t_1)} = \left[\frac{T(t_1)}{T(t_2)}\right]^{3/2}. \tag{4}$$

The ratio $V_l(t_2)/V_l(t_1)$ is ~0.7, while the ratio $\eta(t_2)/\eta(t_1)$ is ~0.6. The change in V_l can be attributed almost entirely to

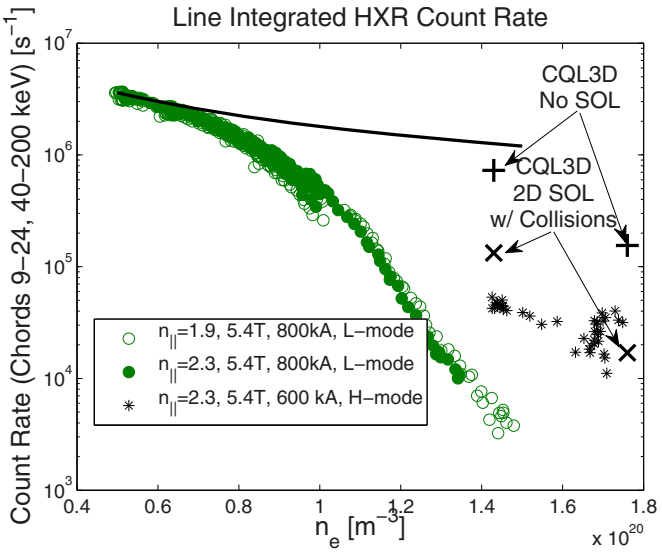

FIG. 17. (Color online) HXR emission as a function of line averaged density during H-mode. Small black data points show experimental data in H-mode, while large black data points represent simulated emission from GENRAY/CQL3D. 800 kA, 5.4 T L-mode data are included for reference.

the increase in plasma temperature, not due to direct current driven by the LH waves. Although this analysis shows that little or no current is directly driven by LHCD in this discharge, the changes in the plasma discussed above demonstrate that LHCD applied to H-modes can have a substantial positive effect on the plasma even above the observed density limit for L-modes.

When the SOL is included in the model of the H-mode discharges, the ray trajectories dwell considerably outside the separatrix both before and after the profiles are modified by LHCD. As with the high density L-mode discharges, even rays that are not trapped outside the separatrix do not penetrate far into the core plasma.

The discrepancy between experimental data and the predictions from CQL3D is smaller for H-mode than for L-mode, even with no SOL model or collisional damping included in GENRAY, as seen in Fig. 17. This suggests that the density limit is sensitive to the specifics of the SOL profiles as opposed to a simple "critical density." Figure 17 also shows the results of simulations with a 2D SOL model including collisions compared with the experimental results. As with the L-mode discharges, including both the SOL and collisional damping improves agreement between the experiment and the simulations considerably.

V. DISCUSSION AND CONCLUSIONS

Experimental observations of fast electron bremsstrahlung emission show that the fast electron population in L-mode plasmas is significantly reduced at line averaged densities above 1×10^{20} m^{-3}. Electric currents measured in the SOL rise sharply at approximately the same density. Taken together, this suggests that the LH waves are depositing their energy outside the separatrix. "Density limits" for effective LHCD have been observed on previous experiments, although the observed limit on C-Mod is significantly lower than the predicted limit based on prior results.

Explanations for previously observed density limits, such as PDI and accessibility criterion violation, disagree with the phenomenology of the C-Mod limit. The sudden drop in fast electrons at high density is not predicted by conventional ray tracing/Fokker–Planck models. By adding the effects of collisional absorption in the SOL to these models, the agreement with experiment at high density is significantly improved. Based on interpretation of the modeling results, the lack of fast electrons at high density is caused by a confluence of several effects. The high density prevents waves from penetrating deep into the hottest part of the plasma and also lowers the overall temperature of the plasma. This reduces single-pass absorption, which is weak even at low density for $n_{||} \leq 2.33$. When combined with an edge loss mechanism, the weak damping inside the separatrix leads to more transits of the rays to the edge, resulting in the absorption of wave power outside the separatrix via collisional damping. The result could theoretically be mitigated by either reducing the edge loss mechanism or increasing core damping. The increased temperature of H-mode plasmas strengthens core absorption although no experimental means of eliminating the edge losses has yet been identified on C-Mod short of operating at lower density.

Increasing the electron temperature on closed flux surfaces, particularly in the outer part of the plasma $(r/a > 0.7)$, may increase single-pass absorption in L- and I-mode[31] discharges, thereby reducing parasitic edge losses incurred after the first pass. The temperature and density profiles in the SOL could also be adjusted by varying the connection length in the SOL and the plasma topology. Future experimental work will focus on these avenues of research along with better characterization of the driven current profile with stationary plasma profiles.

These results highlight the importance of treating the edge and core propagation/absorption problems simultaneously. The disconnect between edge coupling, treated by coupling codes such as GRILL (Ref. 32) or ALOHA,[33] and core propagation/absorption, treated by traditional ray tracing/Fokker–Planck codes such as GENRAY/CQL3D, must be bridged and the two problems treated together. Recent advances in full wave simulations with codes such as TORIC-LH (Refs. 34 and 35) and LHEAF (Refs. 36 and 37), allow proper treatment of wave propagation in the vicinity of the cutoff layer where the WKB approximation is not well satisfied. It is imperative to consider not only the power leaving the antenna but also the power actually absorbed on closed flux surfaces when simulating tokamak plasmas in the low single-pass absorption regime.

ACKNOWLEDGMENTS

The authors would like to thank the C-Mod LHCD engineering team for their efforts in keeping the system running.

This work supported by US DOE Award Nos. DE-FC02-99ER54512 and DE-AC02-76CH03073.

[1]P. T. Bonoli, R. Parker, S. J. Wukitch, Y. Lin, M. Porkolab, J. C. Wright, E. Edlund, T. Graves, L. Lin, J. Liptac, A. Parisot, A. E. Schmidt, V. Tang, W. Beck, R. Childs, M. Grimes, D. Gwinn, D. Johnson, J. Irby, A. Kanojia, P. Koert, S. Marazita, E. Marmar, D. Terry, R. Vieira, G. Wallace, J. Zaks, S. Bernabei, C. Brunkhorse, R. Ellis, E. Fredd, N. Greenough, J. Hosea, C. C. Kung, G. D. Loesser, J. Rushinski, G. Schilling, C. K. Phillips, J. R. Wilson, R. W. Harvey, C. L. Fiore, R. Granetz, M. Greenwald, A. E. Hubbard, I. H. Hutchinson, B. LaBombard, B. Lipschultz, J. Rice, J. A. Snipes, J. Terry, S. M. Wolfe, and Alcator C-Mod Team, Fusion Sci. Technol. **51**, 401 (2007).
[2]I. H. Hutchinson, R. Boivin, F. Bombarda, P. Bonoli, S. Fairfax, C. Fiore, J. Goetz, S. Golovato, R. Granetz, M. Greenwald, S. Horne, A. Hubbard, J. Irby, B. LaBombard, B. Lipschultz, E. Marmar, G. McCracken, M. Porkolab, J. Rice, J. Snipes, Y. Takase, J. Terry, S. Wolfe, C. Christensen, D. Garnier, M. Graf, T. Hsu, T. Luke, M. May, A. Niemczewski, G. Tinios, J. Schachter, and J. Urbahn, Phys. Plasmas **1**, 1511 (1994).
[3]R. Aymar, P. Barabaschi, and Y. Shimomura, Plasma Phys. Controlled Fusion **44**, 519 (2002).
[4]N. J. Fisch and A. H. Boozer, Phys. Rev. Lett. **45**, 720 (1980).
[5]Y. Takase, M. Porkolab, J. J. Schuss, R. L. Watterson, C. L. Fiore, R. E. Slusher, and C. M. Surko, Phys. Fluids **28**, 983 (1985).
[6]R. Cesario, L. Amicucci, G. Calabrò, A. Cardinali, C. Castaldo, M. Marinucci, L. Panaccione, V. Pericoli-Ridolfini, A. A. Tuccillo, and O. Tudisco, in *Radio Frequency Power in Plasmas: Proceedings of the 18th Topical Conference*, Ghent, 2009, edited by V. Bobkov and J.-M. Noterdaeme (AIP, Melville, 2009), Vol. 1187, pp. 419–422.
[7]M. J. Mayberry, M. Porkolab, K. I. Chen, A. S. Fisher, D. Griffin, R. D. Kaplan, S. C. Luckhardt, J. Ramos, and R. Rohatgi, Phys. Rev. Lett. **55**, 829 (1985).
[8]G. M. Wallace, R. R. Parker, P. T. Bonoli, A. E. Schmidt, D. G. Whyte, J. R. Wilson, and S. J. Wukitch, Bull. Am. Phys. Soc. **53**, 222 (2008).
[9]N. J. Fisch, Rev. Mod. Phys. **59**, 175 (1987).
[10]W. Hooke, Plasma Phys. Controlled Fusion **26**, 133 (1984).
[11]V. E. Golant, Sov. Phys. Tech. Phys. **16**, 1980 (1972).
[12]F. Troyon and F. W. Perkins, in *Proceedings of the Second Topical Conference on RF Plasma Heating*, Lubbock, 1974, edited by R. Dollinger, M. Kristiansen, M. O. Hagler, F. J. Paoloni, and J. Bergstroem (Texas Tech University, Lubbock, TX, 1974), pp. B4.1–B4.6.
[13]M. Porkolab, Phys. Fluids **20**, 2058 (1977).
[14]M. Porkolab, S. Bernabei, W. M. Hooke, R. W. Motley, and T. Nagashima, Phys. Rev. Lett. **38**, 230 (1977).
[15]R. R. Parker, M. Greenwald, S. C. Luckhardt, E. S. Marmar, M. Porkolab, and S. M. Wolfe, Nucl. Fusion **25**, 1127 (1985).
[16]A. P. Smirnov and R. Harvey, Bull. Am. Phys. Soc. **40**, 1837 (1995).
[17]R. W. Harvey and M. McCoy, in *Proceedings of the IAEA Technical Committee Meeting on Simulation and Modeling of Thermonuclear Plasmas*, Montreal, 1992, edited by F. Zacek, J. Stoeckel, J. Badalec, L. Dvoracek, K. Jakubka, P. Kletecka, L. Kryska, P. Magula, J. Mlynar, and F. Soeldner (International Atomic Energy Agency, Vienna, 1992), pp. 489–526.
[18]J. Liptac, R. Parker, V. Tang, Y. Peysson, and J. Decker, Rev. Sci. Instrum. **77**, 103504 (2006).
[19]V. Pericoli-Ridolfini, E. Barbato, S. Cirant, H. Kroegler, L. Panaccione, S. Podda, F. Alladio, B. Angelini, M. L. Apicella, G. Apruzzese, L. Bertalot, A. Bertocchi, M. Borra, G. Bracco, A. Bruschi, G. Buceti, P. Buratti, A. Cardinali, C. Centioli, R. Cesario, S. Ciattaglia, V. Cocilovo, F. Crisanti, R. De Angelis, F. De Marco, B. Esposito, and D. Frigione, Phys. Rev. Lett. **82**, 93 (1999).
[20]M. Porkolab, J. J. Schuss, B. Lloyd, Y. Takase, S. Texter, P. Bonoli, C. Fiore, R. Gandy, D. Gwinn, B. Lipschultz, E. Marmar, D. Pappas, R. Parker, and P. Pribyl, Phys. Rev. Lett. **53**, 450 (1984).
[21]G. Wallace, P. Bonoli, A. Parisot, R. Parker, A. Schmidt, J. R. Wilson, and Alcator C-Mod Team, in *Proceedings of the 17th Topical Conference on Radio Frequency Power in Plasmas*, Clearwater, 2007, edited by P. M. Ryan and D. Rasmussen (AIP, Melville, NY, 2007), Vol. 933, pp. 277–280.
[22]R. McWilliams, E. J. Valeo, R. W. Motley, W. M. Hooke, and L. Olson, Phys. Rev. Lett. **44**, 245 (1980).
[23]B. Labombard, J. A. Goetz, I. Hutchinson, D. Jablonski, J. Kesner, C. Kurz, B. Lipschultz, G. M. McCracken, A. Niemczewski, J. Terry, A. Allen, R. L. Boivin, F. Bombarda, P. Bonoli, C. Christensen, C. Fiore, D. Garnier, S. Golovato, R. Granetz, M. Greenwald, S. Horne, A. Hubbard, J. Irby, D. Lo, D. Lumma, E. Marmar, M. May, A. Mazurenko, R. Nachtrieb, H. Ohkawa, P. O'Shea, M. Porkolab, J. Reardon, J. Rice, J. Rost, J. Schachter, J. Snipes, J. Sorci, P. Stek, Y. Takase, Y. Wang, R. Watterson, J. Weaver, B. Welch, and S. Wolfe, J. Nucl. Mater. **241–243**, 149 (1997).
[24]P. Stangeby, *The Plasma Boundary of Magnetic Fusion Devices* (IOP, Berkshire, 1999).
[25]B. LaBombard, J. Goetz, C. Kurz, D. Jablonski, B. Lipschultz, G. McCracken, A. Niemczewski, R. L. Boivin, F. Bombarda, C. Christensen, S. Fairfax, C. Fiore, D. Garnier, M. Graf, S. Golovato, R. Granetz, M. Greenwald, S. Horne, A. Hubbard, I. Hutchinson, J. Irby, J. Kesner, T. Luke, E. Marmar, M. May, P. O'Shea, M. Porkolab, J. Reardon, J. Rice, J. Schachter, J. Snipes, P. Stek, Y. Takase, J. Terry, G. Tinios, R. Watterson, B. Welch, and S. Wolfe, Phys. Plasmas **2**, 2242 (1995).
[26]P. T. Bonoli and R. C. Englade, Phys. Fluids **29**, 2937 (1986).
[27]G. M. Wallace, R. R. Parker, P. T. Bonoli, R. W. Harvey, A. E. Schmidt, A. P. Smirnov, D. G. Whyte, J. R. Wilson, J. C. Wright, and S. J. Wukitch, in *Radio Frequency Power in Plasmas: Proceedings of the 18th Topical Conference*, Ghent, 2009, edited by V. Bobkov and J.-M. Noterdaeme (AIP, Melville, NY, 2009), Vol. 1187, pp. 395–398.
[28]J. W. Hughes, A. E. Hubbard, G. M. Wallace, M. Greenwald, B. L. LaBombard, L. Lin, R. M. McDermott, R. R. Parker, M. L. Reinke, J. E. Rice, and J. R. Wilson, Nucl. Fusion **50**, 064001 (2010).
[29]B. Lipschultz, Y. Lin, E. Marmar, D. Whyte, S. Wukitch, I. Hutchinson, J. Irby, B. LaBombard, M. Reinke, J. Terry, and G. Wright, J. Nucl. Mater. **363–365**, 1110 (2007).
[30]M. L. Reinke and I. H. Hutchinson, Rev. Sci. Instrum. **79**, 10F306 (2008).
[31]R. M. McDermott, B. Lipschultz, J. W. Hughes, P. J. Catto, A. E. Hubbard, I. H. Hutchinson, R. S. Granetz, M. Greenwald, B. LaBombard, K. Marr, M. L. Reinke, J. E. Rice, and D. Whyte, Phys. Plasmas **16**, 056103 (2009).
[32]M. Brambilla, Nucl. Fusion **16**, 47 (1976).
[33]J. Hillairet, D. Voyer, B. Frincu, O. Meneghini, A. Ekedahl, and M. Goniche, Fusion Eng. Des. **84**, 953 (2009).
[34]J. C. Wright, P. T. Bonoli, C. K. Phillips, E. Valeo, and R. W. Harvey, in *Radio Frequency Power in Plasmas: Proceedings of the 18th Topical Conference*, Ghent, 2009, edited by V. Bobkov and J.-M. Noterdaeme (AIP, Melville, NY, 2009), Vol. 1187, pp. 351–358.
[35]J. C. Wright, P. T. Bonoli, A. E. Schmidt, C. K. Phillips, E. J. Valeo, R. W. Harvey, and M. A. Brambilla, Phys. Plasmas **16**, 072502 (2009).
[36]O. Meneghini, S. Shiraiwa, and R. Parker, Phys. Plasmas **16**, 090701 (2009).
[37]S. Shiraiwa, O. Meneghini, R. Parker, G. Wallace, and J. Wilson, in *Radio Frequency Power in Plasmas: Proceedings of the 18th Topical Conference*, Ghent, 2009, edited by V. Bobkov and J.-M. Noterdaeme (AIP, Melville, NY, 2009), Vol. 1187, pp. 363–366.